remote sensing

MDPI

Article

Swarm Investigation of Ultra-Low-Frequency (ULF) Pulsation and Plasma Irregularity Signatures Potentially Associated with Geophysical Activity

Georgios Balasis [1,*], Angelo De Santis [2], Constantinos Papadimitriou [1,3], Adamantia Zoe Boutsi [1], Gianfranco Cianchini [2], Omiros Giannakis [1], Stelios M. Potirakis [1,4,5] and Mioara Mandea [6]

1 Institute for Astronomy, Astrophysics, Space Applications and Remote Sensing (IAASARS), National Observatory of Athens (NOA), 15236 Athens, Greece; constantinos@noa.gr (C.P.); zboutsi@noa.gr (A.Z.B.); og@noa.gr (O.G.); spoti@uniwa.gr (S.M.P.)
2 Istituto Nazionale di Geofisica e Vulcanologia (INGV), 00143 Rome, Italy; angelo.desantis@ingv.it (A.D.S.); gianfranco.cianchini@ingv.it (G.C.)
3 Department of Physics, National and Kapodistrian University of Athens (NKUA), 15784 Athens, Greece
4 Department of Electrical and Electronics Engineering, University of West Attica (UNIWA), 12244 Athens, Greece
5 Department of Electrical Engineering, Computer Engineering and Informatics, Frederick University, 1036 Nicosia, Cyprus
6 Centre National d'Etudes Spatiales (CNES), 75039 Paris, France; mioara.mandea@cnes.fr
* Correspondence: gbalasis@noa.gr

Abstract: Launched on 22 November 2013, Swarm is the fourth in a series of pioneering Earth Explorer missions and also the European Space Agency's (ESA's) first constellation to advance our understanding of the Earth's magnetic field and the near-Earth electromagnetic environment. Swarm provides an ideal platform in the topside ionosphere for observing ultra-low-frequency (ULF) waves, as well as equatorial spread-F (ESF) events or plasma bubbles, and, thus, offers an excellent opportunity for space weather studies. For this purpose, a specialized time–frequency analysis (TFA) toolbox has been developed for deriving continuous pulsations (Pc), namely Pc1 (0.2–5 Hz) and Pc3 (22–100 mHz), as well as ionospheric plasma irregularity distribution maps. In this methodological paper, we focus on the ULF pulsation and ESF activity observed by Swarm satellites during a time interval centered around the occurrence of the 24 August 2016 Central Italy M6 earthquake. Due to the Swarm orbit's proximity to the earthquake epicenter, i.e., a few hours before the earthquake occurred, data from the mission may offer a variety of interesting observations around the time of the earthquake event. These observations could be associated with the occurrence of this geophysical event. Most notably, we observed an electron density perturbation occurring 6 h prior to the earthquake. This perturbation was detected when the satellites were flying above Italy.

Keywords: space weather; earthquake; Swarm satellites; time–frequency analysis; earth observation

Citation: Balasis, G.; De Santis, A.; Papadimitriou, C.; Boutsi, A.Z.; Cianchini, G.; Giannakis, O.; Potirakis, S.M.; Mandea, M. Swarm Investigation of Ultra-Low-Frequency (ULF) Pulsation and Plasma Irregularity Signatures Potentially Associated with Geophysical Activity. *Remote Sens.* **2024**, *16*, 3506. https://doi.org/10.3390/rs16183506

Academic Editors: Changbao Guo, Michele Saroli, Matteo Albano and Ping Lu

Received: 22 July 2024
Revised: 6 September 2024
Accepted: 18 September 2024
Published: 21 September 2024

1. Introduction

The ongoing Swarm mission of the European Space Agency (ESA) provides an opportunity for more detailed knowledge of the Earth's magnetic field and the near-Earth electromagnetic environment. Swarm is the first constellation mission of ESA's Earth Explorers [1]. The constellation consists of three identical satellites, a lower pair (A and C), which are positioned "side by side" with a nominal 150 km separation at the equator and a 4–10 s along-track separation to avoid collision at the poles, and an upper satellite (B) in a nominally different local time orbit. The final configuration of the three-satellite mission, with two spacecraft (Swarm A and C) flying side-by-side at a low altitude (∼460 km) and one spacecraft (Swarm B) flying at a slightly higher altitude (∼510 km), was achieved on 17 April 2014. For our analysis, we used magnetic field data from the vector fluxgate

magnetometer (VFM) on board the three Swarm spacecraft, at 1 Hz cadence. We also processed 2 Hz electron density data from the electric field instruments (EFIs) on board the three satellites. This offers the possibility of investigating ultra-low-frequency (ULF) wave events [2,3]. One of the tools used to analyze these events is time–frequency analysis (TFA). This is a processing tool established for deriving Pc1 (0.2–5 Hz) and Pc3 (22–100 mHz) wave indices [4], but it is also able to detect geophysical signals, due to, for example, plasma instabilities, indicating phenomena such as post-sunset equatorial spread-F (ESF) events or plasma bubbles (see, for instance, ref. [5,6]) and artificial disturbances (anomalies), e.g., spikes and jumps. From a space weather-based point of view, plasma bubbles play a critical role as they can affect global navigation satellite system (GNSS) signals (see, for instance, ref. [7,8]).

ESF events are recognized by sudden depletions in high-electron-density environments. They display a clear seasonal and longitudinal variation in occurrence rates, peaking symmetrically around the dip equator at approximately $\pm 9.5^{\circ}$ magnetic latitude, and extending to $\pm 20^{\circ}$ N [5,9], or possibly even more, depending on factors like solar activity and geomagnetic conditions. ESF events demonstrate a linear relationship with solar extreme ultraviolet (EUV) flux, due to the direct influence of EUV on ionization, thermospheric dynamics, electric fields, and seed perturbations, all of which are critical drivers of ESF activity, and a weak correlation with geomagnetic activity, as indicated by the Kp geomagnetic index (https://www.gfz-potsdam.de/en/section/geomagnetism/data-products-services/geomagnetic-kp-index, accessed on 6 September 2024). Their distribution along longitudes varies with absolute electron density and geomagnetic conditions, with increased occurrence during equinoxes (March and September) and variation during solstices (June and December). High occurrence rates are observed over African and Pacific regions during June, but there is suppression in the Atlantic–American sector and minimal depletions over India [5,9]. In December, the highest ESF rate is over the Atlantic–American region, decreasing westward and eastward. Despite the seasonal variations, ESF events can occur throughout the year, with fluctuations attributed to solar cycle variability. Post-sunset equatorial plasma bubbles (EPBs) contribute to ionospheric irregularities, affecting GNSS signals and other communication systems which rely on quiet ionospheric conditions [7,8]. These irregularities are primarily triggered by the Rayleigh–Taylor instability, which enhances the gradient at the F-layer's bottom side. However, despite the well-established climatological patterns of EPBs, their predictability remains challenging due to day-to-day variability and storm-time behavior.

A few previous studies have suggested that ULF magnetic fields may be associated with earthquakes [10,11]. The majority of these studies refer to the detection of these signals using ground-based magnetometer measurements ([12,13] and references therein). Ground-based electromagnetic observations at several different bands have provided multiple pieces of evidence of possible earthquake-related anomalies at various lead times. Among them, the most intensively investigated are as follows: (a) seismic electric signals (SESs) (<1 Hz), which are geoelectric signals ([14] and references therein); (b) ULF magnetic field anomalies, some of which are attributed to direct emissions from the lithosphere, whereas others are likely to be related to seismogenic perturbations in the lower ionosphere (depression in the horizontal ULF magnetic field), e.g., [12,13,15,16]; (c) ULF/extremely low- frequency (ELF) (3 mHz–40 Hz) atmospheric electromagnetic radiation ([16,17] and references therein); (d) fracture-induced electromagnetic emissions (FEME) (also known as fracture-induced electromagnetic radiation, FEMR), successively emerging in the MHz and kHz bands ([18–20] and references therein); (e) very low frequency/low frequency (VLF/LF) sub-ionospheric propagation anomalies [21,22]; and (f) ionospheric anomalies using ionosonde sounding, e.g., [23,24].

On the other hand, there had only been a handful of studies that attempted to correlate ULF pulsations with seismic activity from spaceborne measurements before the Swarm era, e.g., [25] for the CHAMP satellite and [26] for the DEMETER satellite. Following the launch of the Swarm satellites, there has been an increasing number of studies (e.g., [27,28]

and references therein) on the near-Earth electromagnetic environment associated with the lithosphere–atmosphere–ionosphere coupling (LAIC). For instance, De Santis et al. [27] analyzed Swarm data around the time of the Nepal earthquake (M7.8), which occurred on 25 April 2015. The comparison of the Pc3 wave power levels during the same two-month period over three years (the earthquake year, together with the previous year and the following year) showed clear differences in the region around the earthquake's epicenter. In [28], the authors performed an intensive and systematic analysis of Swarm satellite magnetic field and electron density measurements all over the world from 1 January 2014 to 31 August 2018, and compared the results with M5+ earthquakes occurring in the same period. Applying the superposed epoch and space approach, they found a robust statistical correlation between pre-earthquake anomalies and earthquakes. The occurrence of anomalies were in almost all pre-earthquake period of 90-day investigation, and some occurred even on the same day of the earthquake. This paper also confirmed the Rikitake law [29], relating the earthquake's magnitude and the precursor time, a law that was initially found to apply to ground data, including electromagnetic data. De Santis et al. [30] applied a multiparametric and multilayer approach to the study of the 6 July 2019 M7.1 Ridgecrest earthquake. Many parameters, from the lithosphere to the atmosphere and the ionosphere, were used. Regarding the magnetic field measured by the Swarm satellites, some groups of anomalies were detected, in particular 150, 70–65, and 35–25 days before the earthquake. Interestingly, there was an astonishing agreement in the cumulative number of lithospheric anomalies and of atmospheric and ionospheric anomalies, supporting the hypothesis that the lithospheric activity was the main driver of atmospheric and ionospheric anomalies. Both [29,30] are very good examples that the Swarm satellite magnetic field and electron density measurements can complement ground-based observations, underlying the great importance of this satellite data analysis.

In this study, we focus on the ULF pulsation and ESF activity observed by Swarm satellites during a time interval centered around the occurrence of the August 2016 Central Italy earthquake, which had a 6.0 moment magnitude and hit Central Italy on 24 August 2016. Because the Swarm's orbit was in close proximity to the earthquake epicenter, with Swarm crossing Italy approximately 6 h before the earthquake occurred (see Figure 1), data from the mission may offer valuable observations from that time. These observations could be associated with the occurrence of this geophysical event.

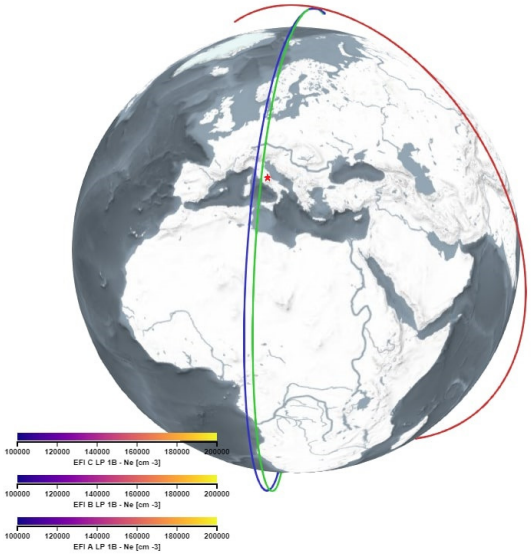

Figure 1. VirES web interface (https://vires.services, accessed on 6 September 2024): globe view and 3D visualization of Swarm orbit on 23 August 2016 from 19:14 to 20:00 coordinated universal time (UTC). Swarm A's track is depicted in blue, Swarm C's track is depicted in green, and Swarm B's track is in red. The red star shows the epicenter of the August 2016 Central Italy earthquake. Swarm A and C flew above the epicenter 6 h prior to the occurrence of the earthquake.

This paper is organized as follows. Section 2.1 presents the data from and the geomagnetic activity during the time interval considered, while Section 2.2 describes the characteristics of the tool set applied to analyze these data. The rest of the paper presents the obtained results from applying the TFA toolbox to data around the time of the Central Italy Earthquake (Section 3) and finishes with some discussions and conclusions (Section 4).

2. Materials and Methods

2.1. Data Description and Geomagnetic Activity Conditions

The August 2016 Central Italy earthquake (epicenter: 42.71° latitude, 13.17° longitude) had a 6.0 moment magnitude and hit Central Italy on 24 August 2016 at 03:36:32 central European summer time (CEST) (01:36 UTC), displaying a focal mechanism consistent with extensional kinematics and a minimum stress axis oriented perpendicular to the Apenninic chain's axis [31]. Its epicenter was close to Accumoli, with its hypocenter at a depth of 4 ± 1 km, approximately 75 km southeast of Perugia and 45 km north of L'Aquila, in an area near the borders of the Umbria, Lazio, Abruzzo, and Marche regions.

In this study, we focus on the ULF pulsation and ESF activity observed by Swarm satellites. The temporal window we have chosen is centered around the seismic event, with a fortuitous alignment of Swarm satellites passing over the geographical location of the earthquake epicenter a few hours prior to the earthquake. Such synchronous positioning of the Swarm constellation above the affected region is an infrequent circumstance and the analysis of the specific datasets could provide valuable insight regarding irregular signal signatures that precede strong geophysical activity.

Regarding Swarm magnetic field measurements, the mission offers 1 Hz absolute scalar magnetometer (ASM) data, as well as 1 Hz and 50 Hz vector field magnetometer (VFM) data. Furthermore, there is an ASM burst mode that offers 250 Hz ASM data for selected time intervals. Regarding Swarm in situ ionospheric electric field and plasma measurements [32], the mission offers 2 Hz electron density data collected from the Langmuir probe component of the electric field instrument (EFI). Regarding wave investigation with Swarm, the mission can detect ULF waves (at the Pc1 and Pc3 frequency ranges), but also the ELF portion of whistler waves (10–120 Hz band) detected during ASM burst mode sessions [33]. The Swarm TFA toolbox could, in principle, investigate all the above-mentioned types of waves detected with instruments onboard the mission (see also Section 2.2 for more details). Therefore, an inherent limitation of the tool may be considered that it is bound to analyze specific frequency ranges due to the cadence constraints imposed by the mission payload.

Figure 1 has been produced using the VirES web interface (https://vires.services, accessed on 6 September 2024). VirES for Swarm is an advanced platform tailored for the effective manipulation and retrieval of data pertinent to Swarm. VirES includes tools for studying various geomagnetic models by comparing them to real-time measurements obtained from the Swarm satellites, providing a comprehensive understanding of Earth's magnetic field dynamics under specific space weather and ionospheric conditions. In this specific 3D visualization of the globe, the tracks of the three Swarm satellites are shown, with the lower pair of satellites flying above Italy right before (i.e., approximately 6 h before) the occurrence of the August 2016 earthquake. Specifically, the track expands from approximately 19:15 UTC to 20:00 UTC on 23 August 2016. In Appendix A, supplementary to Figure 1, we present additional satellite tracks observed before and after the depicted trajectory of Figure 1. These supplementary tracks serve to delineate the longitudinal positions of the satellites relative to the Earth's surface and to evidence the uniqueness of the track over the epicentral region.

Regarding the geomagnetic activity conditions around the time of the earthquake, we have examined the hourly disturbance storm-time (Dst) index (https://wdc.kugi.kyoto-u.ac.jp/dstdir/, accessed on 6 September 2024). The Dst index denotes the mean variation in the horizontal component of Earth's magnetic field, as observed at four mid-latitude magnetic observatories. This variation is attributed to enhancements in the magnetospheric ring current encircling the Earth, thereby serving as a proxy of magnetic storm intensity.

In Figure 2, we show the Dst index for the month of August 2016. On 23 August 2016 at 22:00 UTC, the Dst index reached a minimum value of −73 nT, indicating a moderate magnetic storm [34]. This event was recorded a few hours (i.e., approximately 3.5 h) before the occurrence of the earthquake in Central Italy.

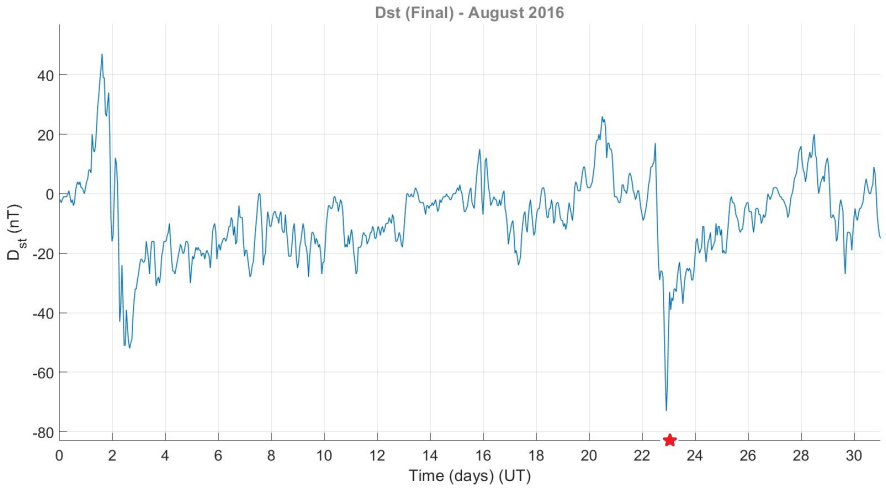

Figure 2. On the 23rd of August, 2016, at 22:00 UTC, the Dst index reached −73 nT, indicating a moderate magnetic storm. The red star shows the time of occurrence of the earthquake.

2.2. The Swarm Time–Frequency Analysis (TFA) Toolbox

For the self-consistency of this paper, let us provide a few details about TFA. The TFA tool is a MATLAB code that includes a graphical interface, as well as a dedicated back end, that can be used to perform wavelet analysis and visualize the results for both Pc1 and Pc3 waves, using both Swarm magnetic field Level 1b 50 Hz and 1 Hz data [4]. Following recommendations from the Advisory Board of the Swarm Data, Innovation and Science Cluster (Swarm DISC), the tool has been further developed. It has also been generalized to accommodate the analysis of other types of time series from both satellite and ground station measurements. In particular, the resulting TFA toolbox provides users with the ability to study different wave types (e.g., compressional waves, Alfvén waves, etc.), various magnetic field components (e.g., mean field aligned (MFA) coordinates), and other geophysical measurements (e.g., electric field and plasma parameters). The TFA toolbox is also able to detect ESF signature events and artificial noise. It is also possible to analyze data from ground stations in a consistent format using TFA, e.g., 1 Hz magnetic observatory data, as available in the virtual research service, VirES for Swarm. Moreover, parts of the TFA toolbox have been integrated into the Python SwarmPAL module (https://swarmpal.readthedocs.io/, accessed on 6 September 2024) and are continuously being developed and upgraded.

Figure 3 shows the graphical interface of the MATLAB version of the tool, with the input parameters displayed as drop-down menus on the left panel of the screen and the results of the analysis presented in the right panel. The typical outputs are composed of three rows of plots; the top one comprises the time series of the (processed and filtered) magnetic field, the middle comprises the image of the wavelet power spectrum for the given range of frequencies, and the bottom row plots the electron density (green line) and the satellite's magnetic latitude in the same graph. All panels correspond to the same time interval. Additional columns can be used to plot the analysis results of other components of the magnetic field from the same satellite, or the same component (or total field) from another satellite of the Swarm constellation.

Examples of the four types of events identified by the TFA tool are shown in Figure 4. A true ULF event will resemble the image in the top left panel, where strong wavelet power is displayed continuously for a long time interval, while also being bounded from top and bottom, i.e., having the entirety of its activity within the frequency range that was

indicated. ESF events have a similar signature in the wavelet images, but they are typically composed of two parts, which are symmetric around the magnetic equator and often look like mirror images of one another. Their detection usually requires additional information from the electron density time series that exhibits rough variations during such events. One example is shown in the top right panel of Figure 4. Other types of signals are the ones produced due to spikes or discontinuities in the data. These produce short, broadband signatures in the data that are easily identified as such and are classified as artificial signals that should not be mixed with other signals of physics-based origins (bottom left panel). Lastly, when no wave activity of any kind is present, the wavelet spectra are characterized as background noise (bottom right panel of Figure 4).

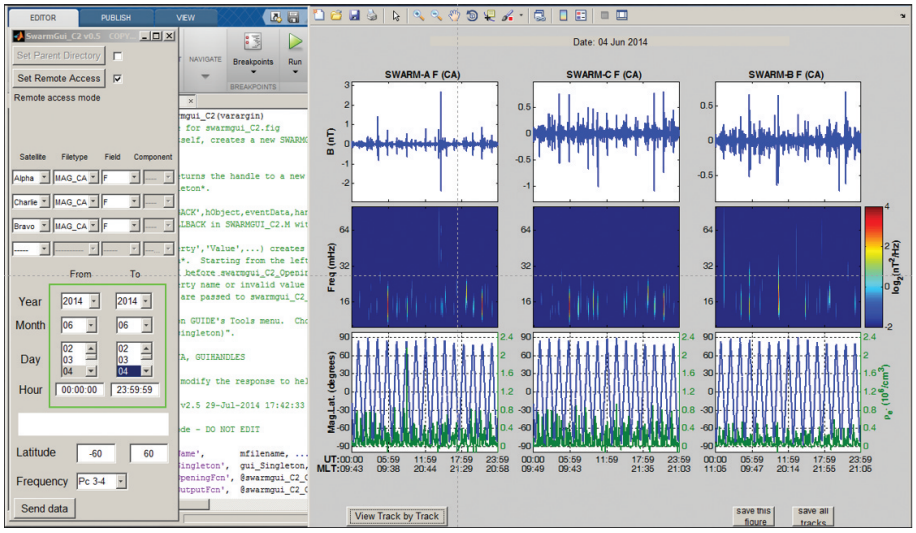

Figure 3. TFA tool environment. From left to right: the user interface, the backend of the tool and the plotter. Here, the plots show the magnetic field B, the frequencies (corresponding to Pc 3–4 ULF waves), and the magnetic latitudes, as measured by Swarm A, C, and B, respectively, on 4 June 2014.

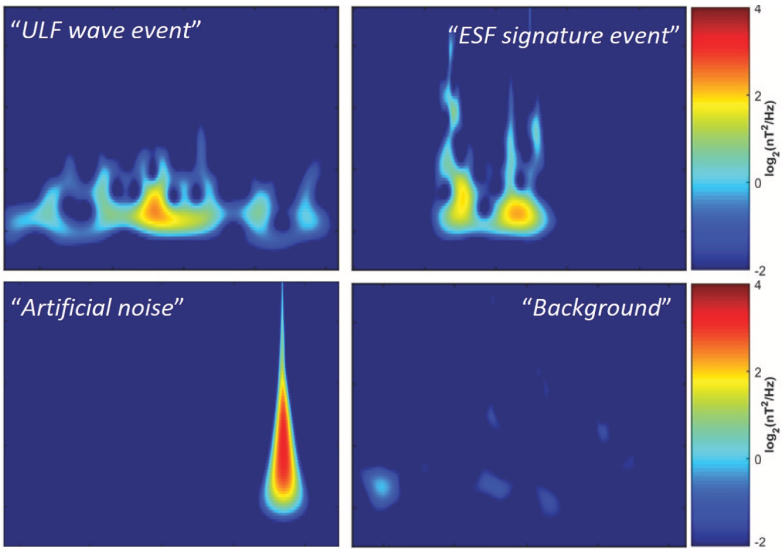

Figure 4. The four distinct categories of signals encountered in the Swarm time series, as seen in the wavelet domain using the TFA tool: "Pc3 ULF wave events" (top left), "ESF signature events" (top right), "Artificial noise" (bottom left), and "Background noise" (bottom right).

The user provides as inputs a start and end date/time, a chosen satellite, and a selected component of the magnetic field (or its total vector magnitude). The magnetic field data are retrieved automatically from ESA's Swarm File Transfer Protocol (FTP) repository, not

only for the specified interval, but also for a few hours prior and after it. This is necessary because the wavelet analysis, like most spectral methods, requires the analyzed signal to be periodic. If it is not, then edge effects emerge at the beginning and end of the analyzed interval that need to be removed, which in this case is achieved by introducing a few extra hours of signal that, in the end, can be safely removed from the process. After the data retrieval, the CHAMP, Ørsted, and Swarm field model (CHAOS) internal part [35] is subtracted from the data, to keep only the magnetic field component that is caused by space weather phenomena, and the new residual time series is high-pass filtered to remove the longer time-scale variations and bring into focus the requested frequency range (Pc3, Pc2 or Pc1). It is on this filtered signal that the wavelet transform is applied [36] and the wavelet power (squared magnitude) is plotted in the time–frequency domain. Ancillary data like the satellite's magnetic latitude and the electron density are also retrieved, for the same time period, and plotted along with the wavelet spectrum. After the analysis is complete, the tool provides an additional option to view the results in a track-by-track fashion, i.e., to see the plots that correspond to each half orbit of the satellite, navigate to the next/previous one and save all such figures on disk.

3. Results

In Figures 5–8 we present the wavelet spectra of the Swarm magnetic field recordings, along with Swarm electron density variations analyzed using the TFA toolbox. Figures 5–8 represent four ascending satellite tracks covering the time interval from 17:41 to 23:06 UTC on 23 August 2016. The considered time interval includes a track when Swarm A and C satellites were flying above Italy, i.e., 6 h before the occurrence of the 24 August 2016 Central Italy earthquake. Six more Swarm ascending tracks, analyzed using the TFA toolbox, are presented in Appendix B: three tracks before and three tracks after this time window.

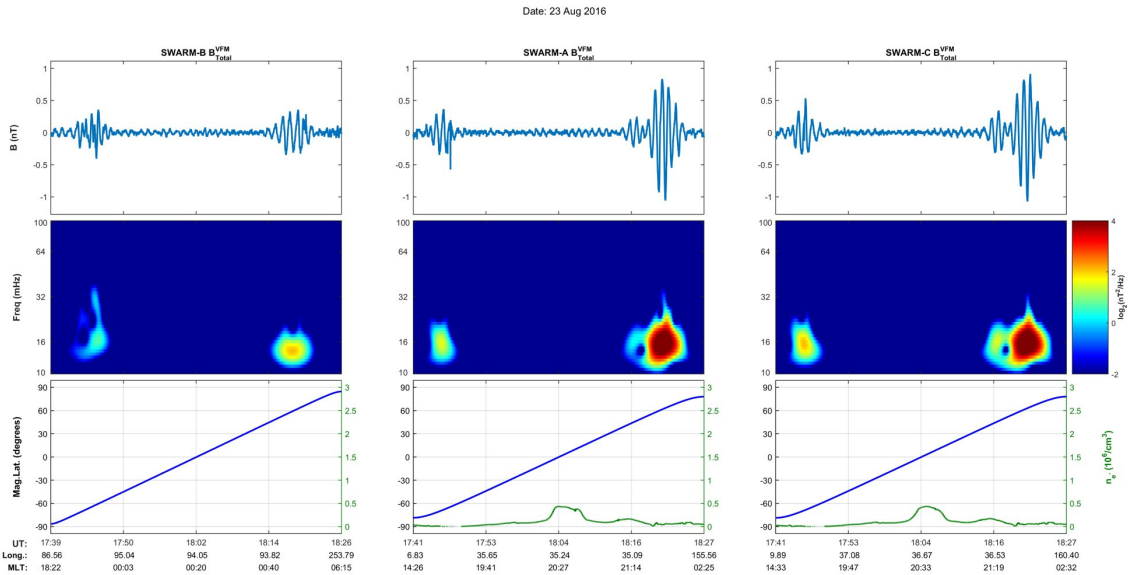

Figure 5. Swarm TFA plot for a full satellite track on 23 August 2016 from 17:41 to 18:27 UTC, before the Central Italy earthquake that occurred on 24 August 2016 at 1:36 UTC. In this track, Swarm A and C fly over Turkey (c.f. Figure A1). (From left to right) Swarm B, A, and C, showing the filtered series of the magnetic field magnitude (top panels), their corresponding wavelet spectra for the joined Pc3 and Pc4 range (middle panels), and a composite plot of the measured electron density (green line) and their location at magnetic latitude (blue line) from -90° to $+90^\circ$ (bottom panels). Please note that, at the bottom of these plots, we provide information on universal time (UT), the geographic longitude, and the magnetic local time (MLT). Apart from the elevated wavelet power of the magnetic field over the north and south poles, no other activity is observed for this track. (Please note, for this and the following tracks, electron density data for Swarm B are unavailable).

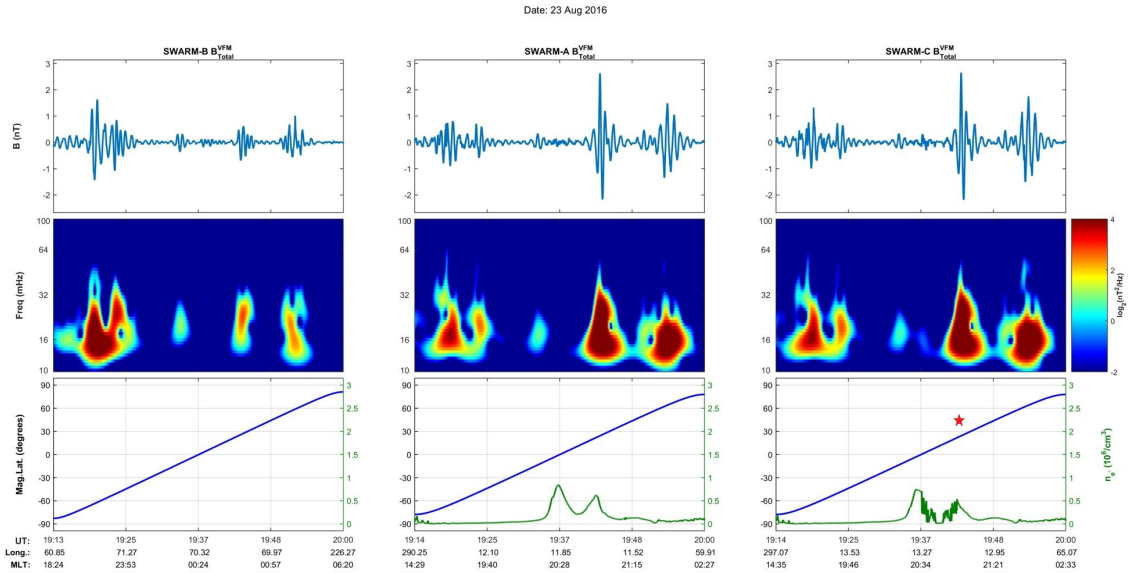

Figure 6. As in Figure 5, for a Swarm track on 23 August 2016 from 19:14 to 20:00 UTC, approximately 6 h before the earthquake. This is the track that Swarm A and C satellites fly over Italy (c.f. Figure 1). Elevated power in the wavelet spectra of the magnetic field is observed in (at least) four distinct areas (including the poles), with more prominent activity for Swarm A and C. Simultaneously, perturbations of electron density are observed at low latitudes only for Swarm C, which was flying closer to the earthquake epicenter than Swarm A. The red star denotes the coordinates of the earthquake epicenter. A question that naturally arises is whether the observed "peculiarity" (i.e., the perturbation seen in the electron density measurements of Swarm C) could be linked to the occurrence of the forthcoming geophysical extreme event.

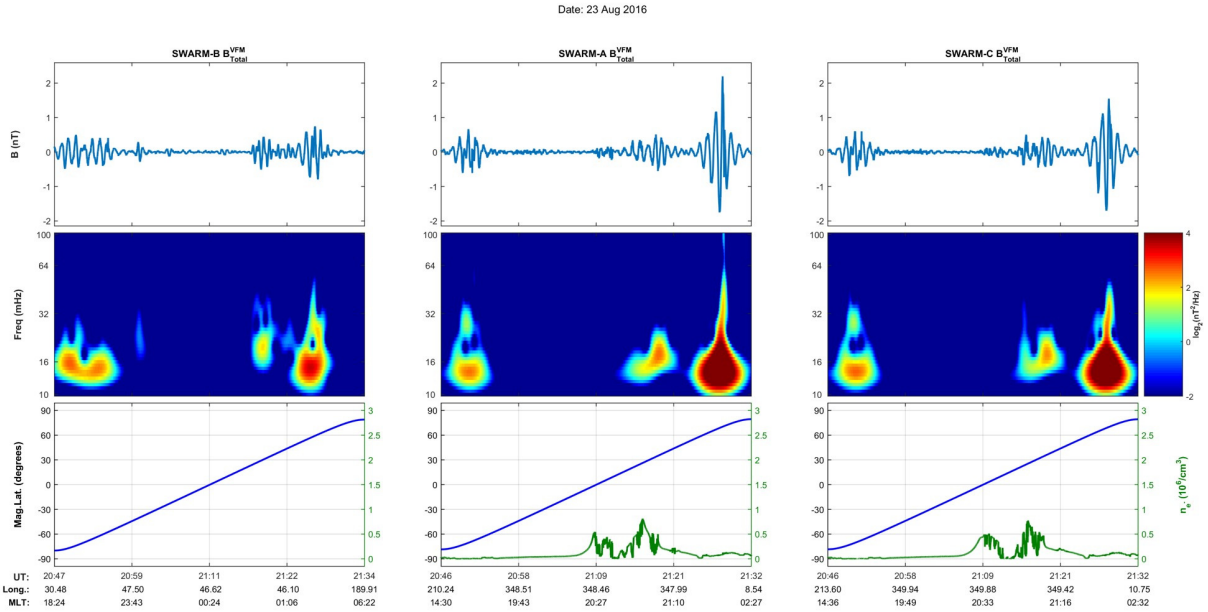

Figure 7. As in Figure 5, for a Swarm track on 23 August 2016 from 20:46 to 21:32 UTC, approximately 4.5 h before the earthquake. However, Swarm A and C satellites fly over the Atlantic ocean (c.f. Figure A2). For Swarm A and C, we observe simultaneous post-sunset perturbations both for the magnetic field and the electron density data at low latitudes. The latter indicates ESF activity. Please note that this track is close temporally (c.f. 30 min before) to the time of the Dst peak value of the magnetic storm shown in Figure 2. As before, we observe increased activity of the magnetic field at auroral latitudes.

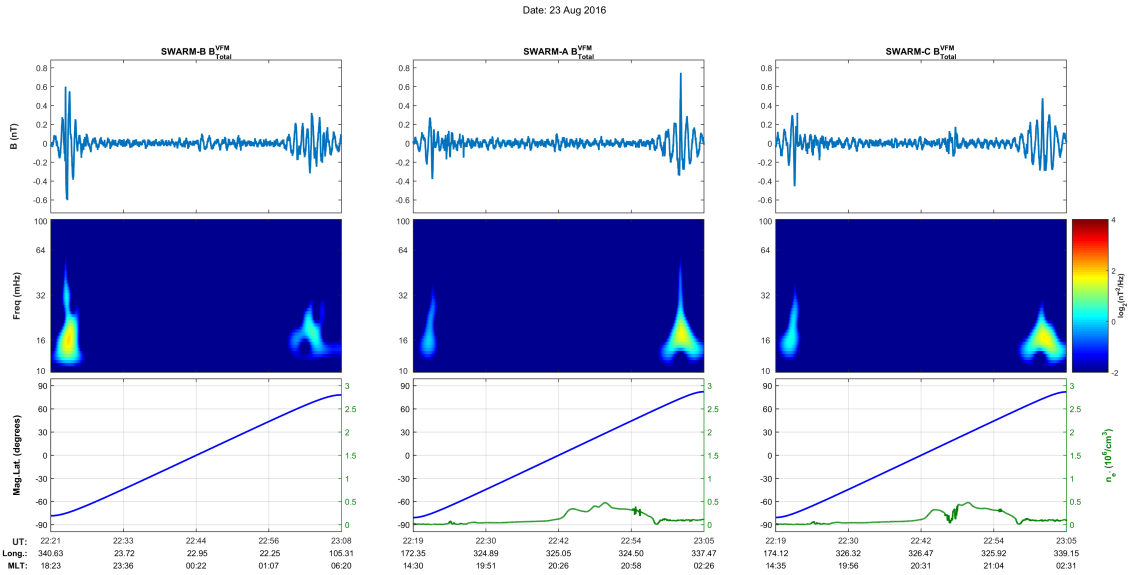

Figure 8. As in Figure 5, for a Swarm track on 23 August 2016 from 22:19 to 23:06 UTC. This track is closer to the time of the earthquake; however, the satellites fly at different distances from the epicenter (c.f. Figure A3). Elevated magnetic field activity is observed only at the poles, while no activity is observed at low latitudes.

Figure 5 presents a Swarm TFA plot for a full satellite track on 23 August 2016 from 17:41 to 18:27 UTC, before the Central Italy earthquake that occurred on 24 August 2016 at 1:36 UTC. In this track, Swarm A and C fly over Turkey (c.f. Figure A1). Swarm B, A, and C (from left to right) show the filtered series of the magnetic field magnitude (top panels), their corresponding wavelet spectra for the joined Pc3 and Pc4 range (middle panels), and a composite plot of the measured electron density (green line) and their location at magnetic latitude (blue line) from -90° to $+90^\circ$ (bottom panels). Apart from the elevated wavelet power over the north and south poles, no other activity is observed for this track (please note that, for this and the following tracks, electron density data for Swarm B are unavailable).

Figure 6 is similar to Figure 5, but for a Swarm track on 23 August 2016 from 19:14 to 20:00 UTC, approximately 6 h before the earthquake. This is the track wherein Swarm A and C satellites fly over Italy (c.f. Figure 1). Elevated power in the wavelet spectra of the magnetic field is observed in (at least) four distinct areas (including the poles), with more prominent activity for Swarm A and C. Simultaneously to the magnetic measurements, perturbations of electron density are observed at low latitudes only for Swarm C, which is flying closer to the area of earthquake epicenter in comparison to Swarm A.

Figure 6 depicts the trajectory followed by Swarm A and C satellites over Italy. Perturbations in electron density are discernible at lower latitudes (i.e., two peaks roughly at -10° and $+15^\circ$ around the equator) however are evident solely in Swarm C data. These observations potentially indicate an ESF event, typically occurring within $\pm 20^\circ$ of the geomagnetic equator. The geographic longitudes associated with this event are approximately 11.85° for Swarm A and 13.27° for Swarm C, whereas the geographic longitude of the earthquake epicenter stands at 13.17°. This likely ESF event transpired in late August, nearly a month preceding the autumnal solstice. As mentioned before, during equinoxes, characterized by maximal solar heating at the equator, ionospheric dynamics are intensified, amplifying the likelihood of ESF occurrences. Remarkably, solar cycle 24 peaked in April 2014, marking the current phase as its declining period. Although periods of heightened geomagnetic activity, such as geomagnetic storms, can perturb the ionosphere and potentially enhance ESF activity, the relationship between geomagnetic activity and ESF events is intricate and not strictly linear.

Figure 7 is similar to Figure 5, but for a Swarm track on 23 August 2016 from 20:46 to 21:32 UTC, approximately 4.5 h before the earthquake. However, Swarm A and C satellites fly over the Atlantic ocean (c.f. Figure A2). For Swarm A and C, we observe simultaneous post-sunset perturbations both for the magnetic field and the electron density data at low latitudes. The latter indicates ESF activity. Please note that this track ends approximately half an hour before the Dst index reaches its peak value for the magnetic storm shown in Figure 2.

In Figure 7, simultaneous post-sunset perturbations in both magnetic field and electron density data are observed at lower latitudes for both Swarm A and C satellites, clearly indicating ESF activity. Analogous to the observations in Figure 6, deviations in electron density are observed within the 0° to +20° range, characteristic of ESF occurrences. The geographic longitudes traversed by Swarm A and C during this event are approximately 348.2° and 349.6°, respectively. As previously noted, this track is close temporally to the time of the Dst peak value of the magnetic storm, thus reflecting a heightened geomagnetic activity as well.

Figure 8 is similar to Figure 5, but for a Swarm track on 23 August 2016 from 22:19 to 23:06 UTC. This track is closer to the time of the earthquake; however, the satellites fly at different distances from the epicenter (c.f. Figure A3). There is an increased wavelet power spectral density; thus, elevated ionospheric activity is observed only at the poles. This track is also very close temporally (approximately 20 min after) to the time of the minimum Dst index value of the moderate magnetic storm that occurred.

4. Discussion and Conclusions

For over more than a decade, the Swarm mission has greatly enhanced our understanding of the physics of the topside ionosphere and of magnetosphere–ionosphere coupling. This includes their corresponding space weather effects.

In this methodologically driven paper, we employ the Swarm time–frequency analysis toolbox to investigate the ultra-low-frequency magnetic activity, as well as the electron density variations, in the ionosphere. Our study focuses on the period around the time of the August 2016 Central Italy earthquake, during which the lower pair of Swarm satellites was crossing Italy. We find several interesting observations of perturbations, including the occurrence of an electron density disturbance at low latitudes in Swarm C's time series, 6 h prior to the earthquake.

Regarding the lead time of a possible earthquake-related electromagnetic signal, we have a large variety of lead times reported in the literature both for ground-based and spaceborne observations. For instance, regarding ground measurements, the SESs, which are accompanied by magnetic field variations in the field vertical component, present a lead-time ranging from a few months to a few weeks before an earthquake's occurrence [14]. Statistical anomalies have been detected from 1–2 months to a few weeks and 2–4 days before an earthquake for the direct ULF magnetic field power and ULF depression, respectively, whereas phase transition characteristics in the raw ULF magnetic field recordings have been identified even a few hours prior to an earthquake's occurrence ([17,37] and references therein). The ULF/ELF pre-seismic anomalies have a lead time of 1 week to 2 days and the VLF/LF sub-ionospheric propagation anomalies have a lead-time of 1 week to 2 days, whereas ionosonde-detected anomalies have been reported as having lead times from 40 days to a few hours [38]. Finally, the MHz FEME/FEMR present a lead time ranging from 2 weeks to a few hours, whereas the kHz FEME/FEMR appear, after the MHz FEME/FEMR, a few days to a few hours before an earthquake's occurrence ([19,20] and references therein).

Let us discuss some of the previously analyzed events and the different conclusions reached using satellite measurements. Marchetti and Akhoondzadeh [39] analyzed Swarm satellite data, including magnetic and electric fields and electron density, on the occasion of the 8 September 2017 M8.2 Mexico earthquake. Around 200 magnetic field anomalies were found in the 5 months before the earthquake. Constructing the cumulative number of these

anomalies, an S-shaped pattern was revealed, with an inflection point about two months before the earthquake. Akhoondzadeh et al. [40] considered several kinds of atmospheric and ionospheric precursors, including Swarm magnetic field data, to the 2016 M7.6 Ecuador earthquake. The analysis of the magnetic field scalar and vector data show considerable anomalies from around 50 to 7 days before the main shock. De Santis et al. [41] analyzed Swarm satellite magnetic field and electron density data one month before and one month after 12 strong earthquakes that occurred in the first 2.5 years of the Swarm satellites' mission lifetime in the Mediterranean region (magnitude M6.1+) or in the rest of the world (M6.7+). They then detected the anomalies using an objective method. Once the anomalies are normalized by the analyzed satellite tracks, they resemble a linear dependence with earthquake magnitude, so supporting a statistical correlation between anomalies and earthquakes and excluding a relationship by chance. In some cases, the anomalies were found also on the day of the earthquake, in particular for the 2015 M7.8 Nepal, the 2016 M7.9 Sumatra, and the 2016 M7 Japan earthquakes.

In Marchetti et al. [42], anomalous magnetic field signals were detected by Swarm satellites during geomagnetically quiet conditions and during major seismic events, from about 4 months before the start of the seismic sequence to the first 8 months after the seismic sequence (i.e., a total of one year of analyzed data). These authors found a very interesting increase in such anomalies, starting about 40 days before the beginning of the seismic sequence, coinciding with and following surface and atmospheric alterations, resulting in a temporal sequence of anomalies from the Earth's surface up to the ionosphere. Akhoondzadeh et al. [43] analyzed three months of global positioning system (GPS) total electron content (TEC) data and four months of Swarm satellite magnetic field, electron density, and temperature data around the time of the 12 November 2017 M7.3 Iran–Iraq earthquake. Regarding the satellite magnetic field anomalies, they found tens of anomalies in the investigated period and reconstructed the cumulative number of anomalies, searching for an S-shaped pattern. An anomaly in total intensity was also found on the day of the earthquake, just before it occurred. Marchetti et al. [44] extended the analysis of Swarm satellite magnetic field data to 1000 days before the 2019 M7.1 Ridgecrest earthquake. They found that some geomagnetic field activity occurred 222 to 168 days before the earthquake, which was anomalous when compared to another confutation area. In addition, the Swarm B satellite passed above the epicentral area 15 min before the earthquake and detected a clear anomaly, mainly in the field east component.

Sasmal et al. [45] analyzed several parameters, including Swarm magnetic field data, during the 30 October 2020 M6.9 Samos (Greece) earthquake. They found a clear anomaly in the vertical component the day before the earthquake. Akhoondzadeh et al. [46] studied several kinds of potential ionospheric precursors before the 14 May 2019 M7.6 Papua New Guinea earthquake, including Swarm magnetic field satellite data. A few tens of magnetic field anomalies were found with a typical S-shape pattern in the four months before the earthquake. Ghamry et al. [47] also found some Swarm magnetic field data anomalies 12 and 13 days before the M7.8 25 April 2015 Nepal earthquake. Zhang et al. [48] studied the pre-occurrence phase of four strong Chinese earthquakes occurring in 2008–2020. They used several ionospheric data from ground and space, including Swarm satellite magnetic field data, for the 2014 and 2020 Yutian earthquakes, and found clear anomalies from two weeks to a week before each earthquake and a few just after. Zhang et al. [49] also analyzed the pre-occurrence phase of the 2022 M6.8 Luding (China) earthquake, by means of a multiparametric and multilayer approach, from ground to atmosphere and ionosphere. Regarding Swarm magnetic field data, they found some anomalies 83, 68, 67, 64, 12, and 11 days before the earthquake. Considering all anomalies with comprehensive accumulation, they recognized a two-way model of LAIC: a slow accelerating trend, which they called the diffusive–thermodynamic coupling, and an intermittent direct coupling, which was probably electromagnetic. Ozsoz et al. [50] analyzed Swarm satellite magnetic field data six months before and one month after five M6+ earthquakes in Turkey and Greece in 2017–2020, finding a few tens of anomalies (they found them when considering

data from all three satellites, so the real number of anomalies would be actually one-third of that total) in the period of study, wherein some earthquakes showed a typical precursory S-shaped pattern (as found for the first time by De Santis et al. [27]).

Interestingly, Heki et al. ([51] and references therein), analyzing the total electron content, i.e., the total number of electrons in the column from the Earth to the satellites (mostly due to the ionospheric electrons), found total electron content anomalies some tens of minutes before a large earthquake; these were times comparable with those of the anomalies found in this work. Notably, our analysis reveals that, preceding and subsequent to the trajectory in question, the satellites traversed disparate longitudinal coordinates. However, during the temporal window corresponding to the capture of the electron density signal, the lower pair of Swarm satellites was coincidentally positioned directly above the geographical region of Italy in question. This fortuitous alignment underscores the spatial–temporal synchronicity between satellite positioning and the occurrence of electron density anomalies, reinforcing the relevance of our findings within the context of geophysical activity and earthquake occurrences.

Our methodology is data-driven, and an anomaly is objectively defined when it is clearly different from the background. We show what we find as something "peculiar" that happens before the M6 earthquake. Although we cannot fully trust it is earthquake-related, there are great chances it is.

It is true that, with some physical consideration relating to the earthquake's magnitude, the size of its preparation area, and the speed of the satellite, a typical anomaly should last about 4–5 min, i.e., a little less time than what we have found. Indeed, according to the Dobrovolksy relationship, the size of the Central Italy earthquake's preparation area was approximately 623 km (in radius) or 1250 km (in diameter), since the seismic sequence culminated with an M6.5 earthquake on 30 October 2016. As the satellite has a typical speed of 7.4 km/s, the time the anomalous area can interact with the ionosphere is of the order of 1250/7.4 = 169 s, which is about 3 min. Considering also the slight enlargement of the Dobrovolsky region when projecting it from the Earth's surface to about 500 km above, in the ionosphere, the larger anomaly cannot last more than 4 min, which is still less than 5–10 min, as we have found. However, we cannot discard a possible distorting and spreading effect of the geomagnetic field and of the atmospheric dynamics, therefore justifying an anomaly lasting 5–10 min.

Another source of concern about the internal geophysical origin of the peculiar signal in the Swarm C time series of electron density data could be that a small concurrent geomagnetic storm was recorded (Figure 1), with the likely source being coronal hole 756, along with a disappearing solar filament. The arrival time of this disturbance is estimated to be around 19:00 on 23 August 2016, which corresponds to the time when the main features in the wavelet spectra of the magnetic field occurred (Figure 6). However, if the peculiar signal had an external origin, it would have been observed simultaneously in both the Swarm A and C time series of electron density data, which is clearly not the case.

The results obtained here pave the way for exploring other types of events using satellite data, as ionospheric processes and the space-based detection of natural hazards continue to be a multidisciplinary research area. The short- and long-term prospects are promising, even though our current understanding of the coupling between the lithosphere, atmosphere, and ionosphere remains limited. This applies not only to the generation of co-seismic and co-volcanic ionospheric disturbances, which are of particular interest, but also to other solid Earth phenomena, such as slow-slip earthquakes and landslides. To enhance our understanding of this complex coupling, it is essential to investigate the formation mechanisms of these ionospheric disturbances. Moreover, a deeper study of how this coupling varies with solar activity levels, atmospheric conditions, and other factors is necessary. In terms of observations, combining electromagnetic measurements with other data, such as high-resolution GNSS or gravity data, is crucial. This combination could provide new insights into the generation and evolution of ionospheric disturbances caused by natural hazard events and how they develop with altitude.

Author Contributions: Conceptualization, G.B. and A.D.S.; methodology, G.B., C.P. and A.Z.B.; software, C.P. and A.Z.B.; investigation, C.P., A.Z.B., G.C. and O.G.; writing—original draft preparation, G.B., A.D.S., C.P., A.Z.B. and S.M.P.; writing—review and editing, A.D.S., G.C., O.G., S.M.P. and M.M. All authors have read and agreed to the published version of the manuscript.

Funding: This study has been supported as part of Swarm DISC (Data, Innovation, and Science Cluster) activities, funded by ESA contract no. 4000109587. Mioara Mandea's work has received funding from the European Research Council (ERC) under the European Union's Horizon 2020 research and innovation program (GRACEFUL Synergy Grant 855677). A.D.S. and G.C. received funds from Italian Space Agency (ASI), Istituto Nazionale di Geofisica e Vulcanologia (INGV), and Ministero dell'Università e della Ricerca (MUR) in the framework of the Limadou+, Lithosphere-Atmosphere-Ionosphere Coupling Analysis (LAICA), and Working Earth (Pianeta Dinamico) Projects, respectively.

Data Availability Statement: The results presented rely on the data collected by the three satellites of the Swarm constellation. Swarm data can be accessed at https://swarm-diss.eo.esa.int/, accessed on 6 September 2024.

Acknowledgments: The authors thank the European Space Agency (ESA) that supports the Swarm mission. The authors acknowledge the Kyoto World Data Center (WDC) for Geomagnetism and the observatories that produce and make the Dst index available at http://wdc.kugi.kyoto-u.ac.jp/, accessed on 6 September 2024.

Conflicts of Interest: The authors declare no conflicts of interest.

Appendix A

Appendix A is supplementary to Figure 1. Here, we provide three additional figures corresponding to the tracks associated with Figures 5, 7, and 8, respectively.

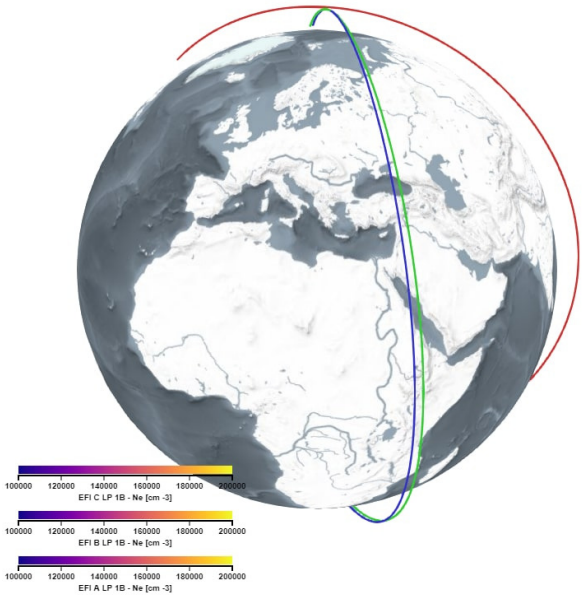

Figure A1. VirES web interface (https://vires.services, accessed on 6 September 2024): globe view with a 3D visualization of Swarm's orbit on 23 August 2016 from 17:41 to 18:27 UTC. Swarm satellites flew above Turkey before capturing an irregular signal (next track, Figure 1) possibly associated with the occurrence of the August 2016 earthquake in Italy. Swarm A's track is depicted in blue, Swarm C's track is depicted in green, and Swarm B's track is depicted in red.

Figure A1 shows the track previous to the one shown in Figure 1 (19:14–20:00), covering the time-frame from 17:41 to 18:27, during which Swarm A and C were flying over Turkey, while Figure A2 shows the subsequent track to Figure 1, expanding from 20:46 to 21:32, in which Swarm A and C were flying over the Atlantic ocean. Finally, Figure A3 shows another subsequent track (22:19–23:06), when none of the Swarm satellites were flying above the epicentral area.

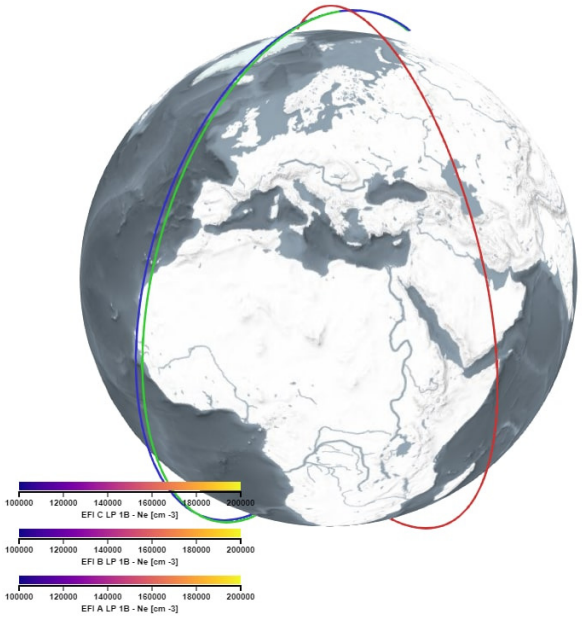

Figure A2. VirES web interface (https://vires.services, accessed on 6 September 2024): globe view and 3D visualization of Swarm's orbit on 23 August 2016 from 20:46 to 21:32 UTC. Swarm satellites flew past Portugal after capturing an irregular signal (previous track, Figure 1) possibly associated with the occurrence of the August 2016 earthquake in Italy. Swarm A's track is depicted in blue, Swarm C's track is depicted in green, and Swarm B's track is depicted in red.

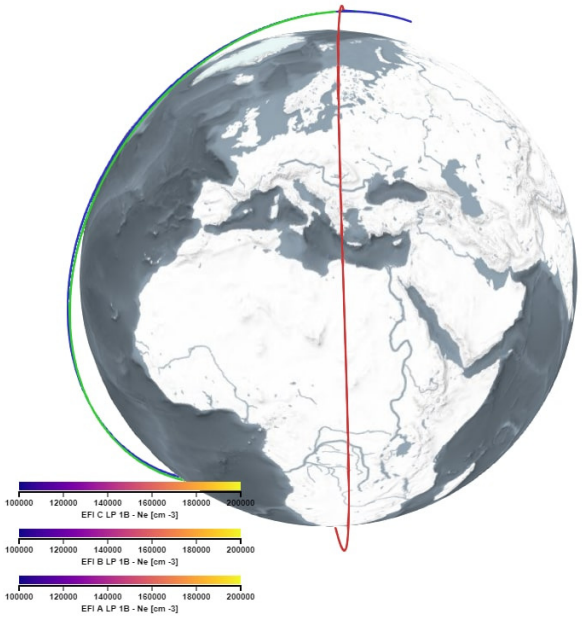

Figure A3. VirES web interface (https://vires.services, accessed on 6 September 2024): globe view and 3D visualization of Swarm's orbit on 23 August 2016 from 22:19 to 23:06 UTC. Swarm satellites flew over the Atlantic ocean after capturing an irregular signal (previous track, Figure A2) possibly associated with the occurrence of the August 2016 earthquake in Italy. Swarm A's track is depicted in blue, Swarm C's track is depicted in green, and Swarm B's track is depicted in red.

Appendix B

Appendix B is supplementary to Figures 5–8. Here, we provide three additional figures corresponding to the ascending tracks before the one shown in Figure 5 and three additional figures corresponding to the ascending tracks after the one shown in Figure 8.

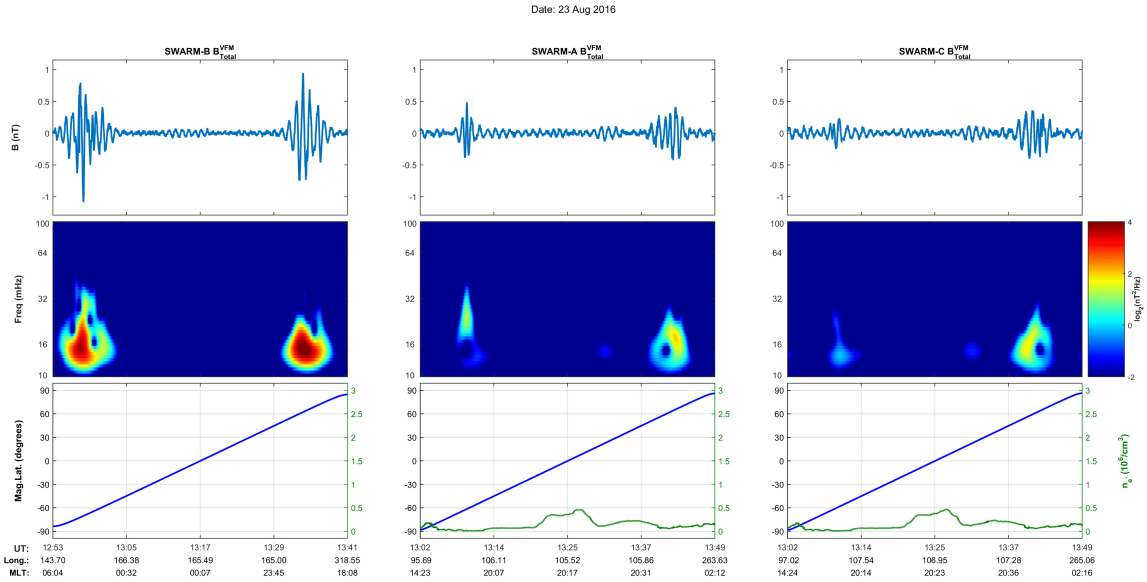

Figure A4. Swarm TFA plot for a full satellite track on 23 August 2016 from 13:02 to 13:49 UTC, before the Central Italy earthquake that occurred on 24 August 2016 at 1:36 UTC. From left to right: Swarm B, A, and C, showing the filtered series of the magnetic field magnitude data (top panels), their corresponding wavelet spectra for the joined Pc3 and Pc4 range (middle panels), and a composite plot of the measured electron density data (green line) and their location at magnetic latitude (blue line) from -90° to $+90^{\circ}$ (bottom panels). Please note that, at the bottom of these plots, we provide information on UT, geographic longitude, and magnetic local time (MLT).

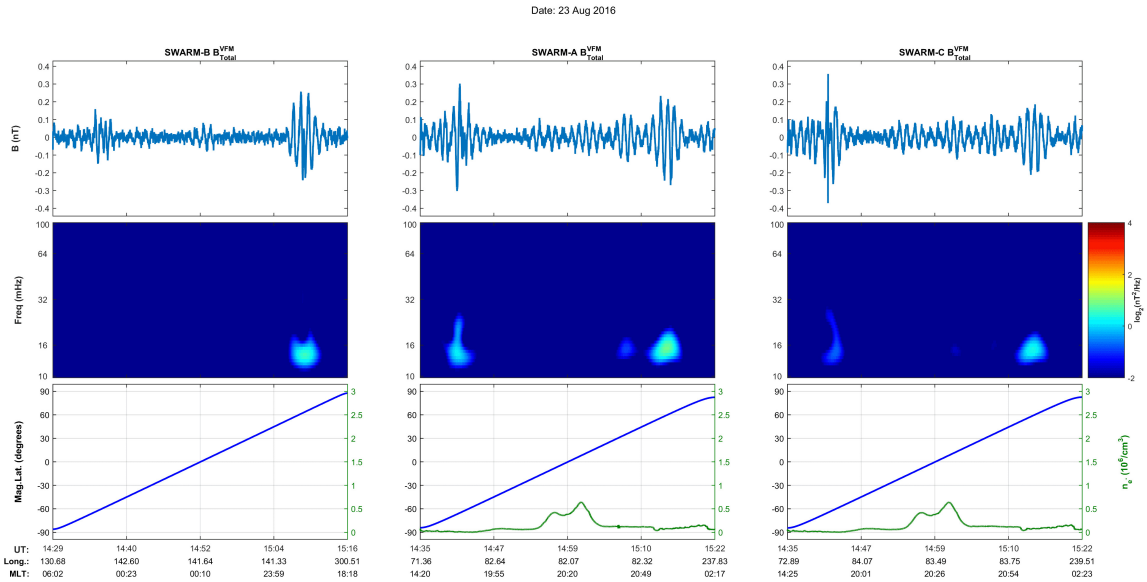

Figure A5. Swarm TFA plot for a full satellite track on 23 August 2016 from 14:35 to 15:22 UTC, before the Central Italy earthquake that occurred on 24 August 2016 at 1:36 UTC. From left to right: Swarm B, A, and C, showing the filtered series of the magnetic field magnitude data (top panels), their corresponding wavelet spectra for the joined Pc3 and Pc4 range (middle panels), and a composite plot of the measured electron density data (green line) and their location at magnetic latitude (blue line) from -90° to $+90^{\circ}$ (bottom panels). Please note that, at the bottom of these plots, we provide information on UT, geographic longitude, and magnetic local time (MLT).

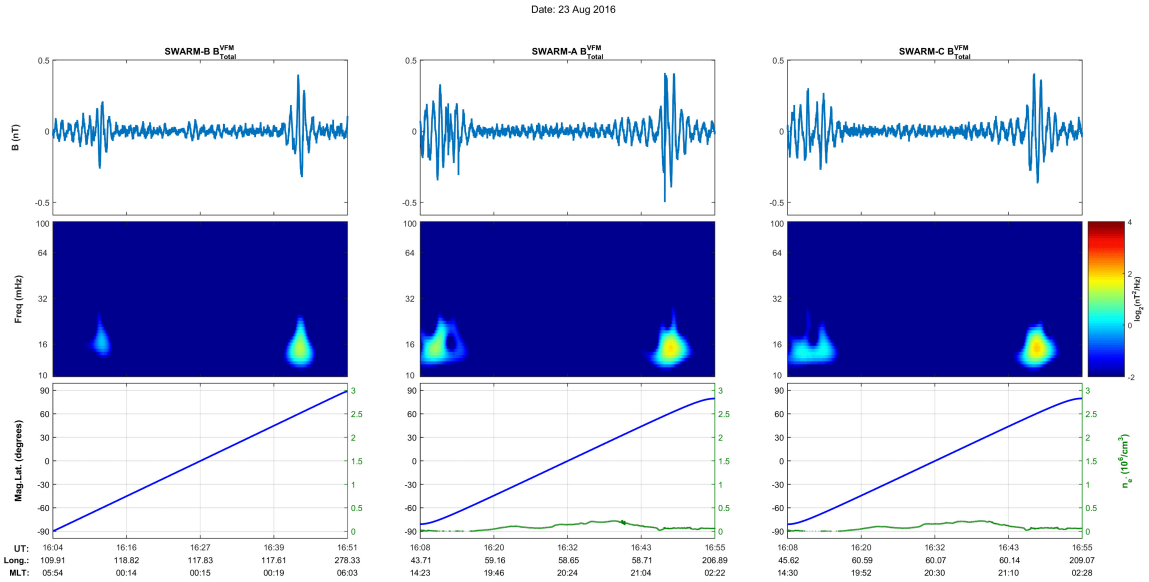

Figure A6. Swarm TFA plot for a full satellite track on 23 August 2016 from 16:08 to 16:55 UTC, before the Central Italy earthquake that occurred on 24 August 2016 at 1:36 UTC. From left to right: Swarm B, A, and C, showing the filtered series of the magnetic field magnitude data (top panels), their corresponding wavelet spectra for the joined Pc3 and Pc4 range (middle panels), and a composite plot of the measured electron density data (green line) and their location at magnetic latitude (blue line) from -90° to $+90^\circ$ (bottom panels). Please note that, at the bottom of these plots, we provide information on UT, geographic longitude, and magnetic local time (MLT).

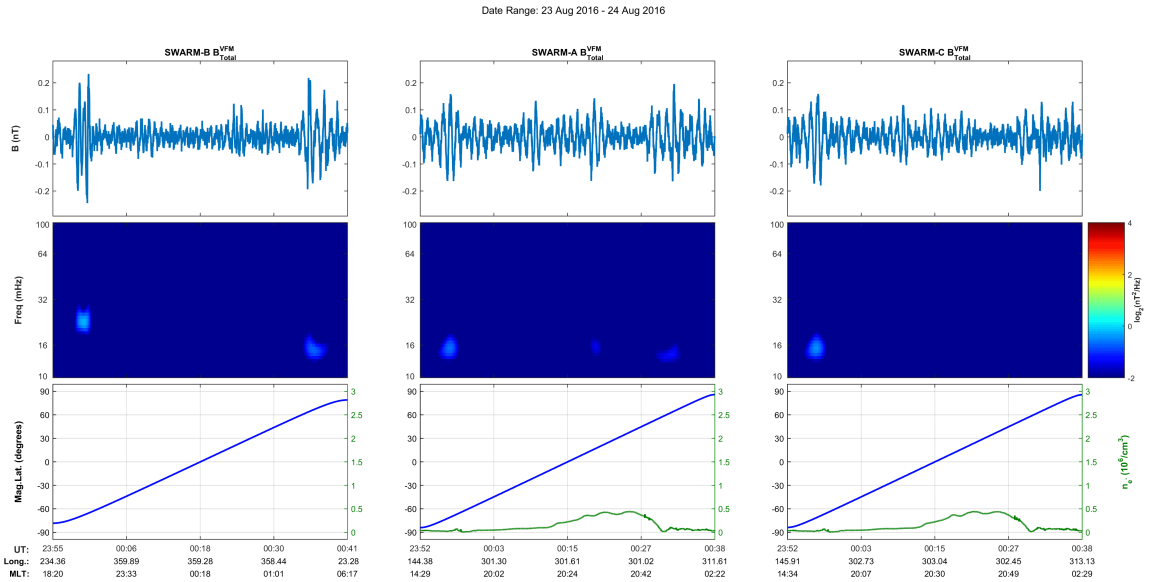

Figure A7. Swarm TFA plot for a full satellite track from 23:52 UTC on 23 August 2016 to 00:58 UTC on 24 August 2016, before the Central Italy earthquake that occurred on 24 August 2016 at 1:36 UTC. From left to right: Swarm B, A, and C, showing the filtered series of the magnetic field magnitude data (top panels), their corresponding wavelet spectra for the joined Pc3 and Pc4 range (middle panels), and a composite plot of the measured electron density data (green line) and their location at magnetic latitude (blue line) from -90° to $+90^\circ$ (bottom panels). Please note that, at the bottom of these plots, we provide information on UT, geographic longitude, and magnetic local time (MLT).

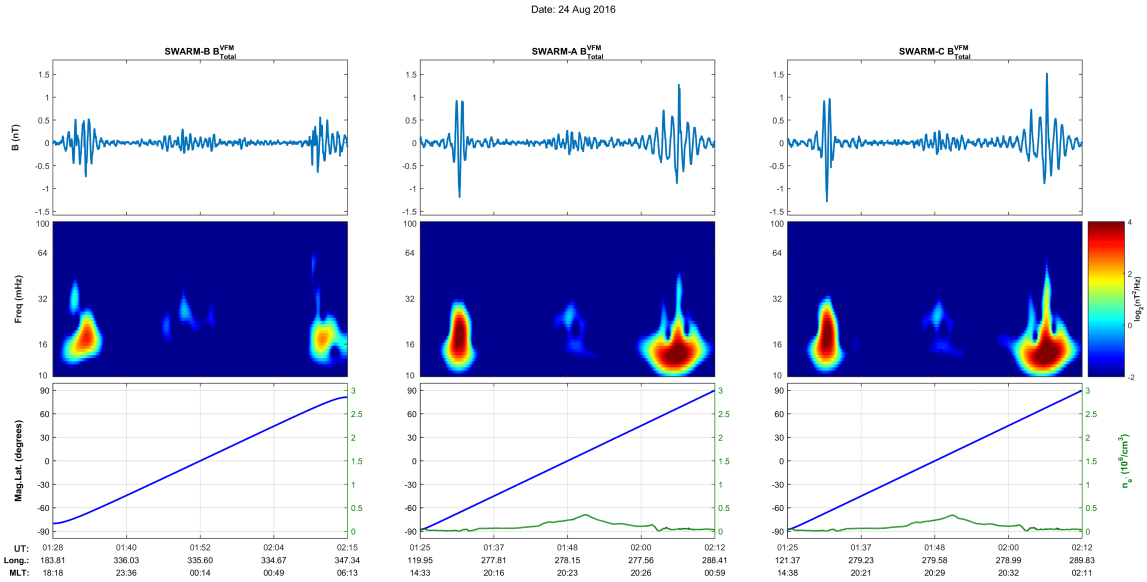

Figure A8. Swarm TFA plot for a full satellite track on 24 August 2016 from 01:25 UTC to 02:12 UTC, before the Central Italy earthquake that occurred on 24 August 2016 at 1:36 UTC. From left to right: Swarm B, A, and C, showing the filtered series of the magnetic field magnitude data (top panels), their corresponding wavelet spectra for the joined Pc3 and Pc4 range (middle panels), and a composite plot of the measured electron density data (green line) and their location at magnetic latitude (blue line) from -90° to $+90^{\circ}$ (bottom panels). Please note that, at the bottom of these plots, we provide information on UT, geographic longitude, and magnetic local time (MLT).

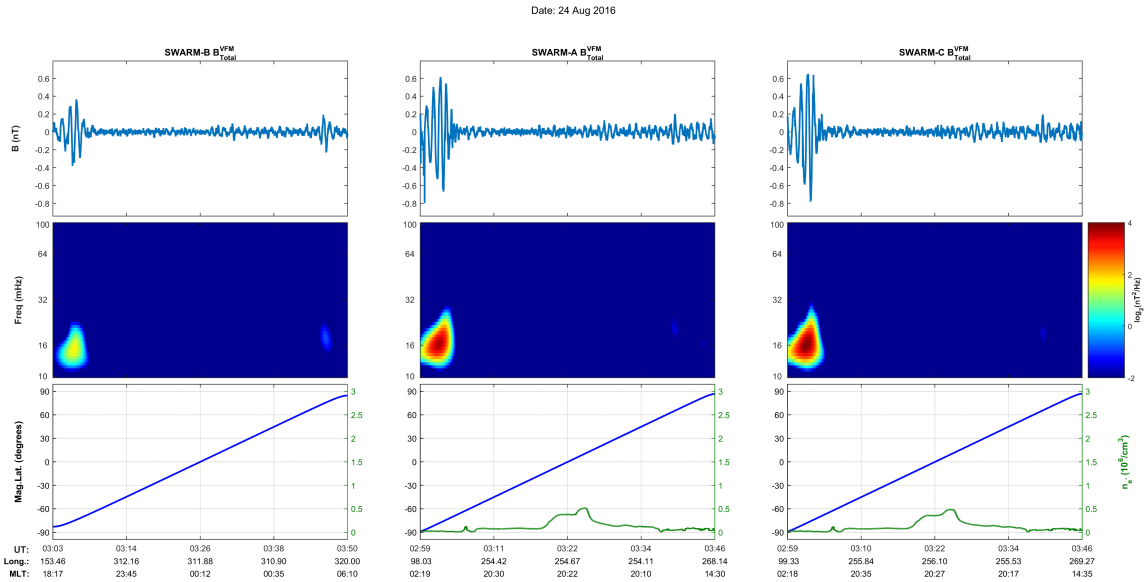

Figure A9. Swarm TFA plot for a full satellite track on 24 August 2016 from 02:59 UTC to 03:46 UTC, before the Central Italy earthquake that occurred on 24 August 2016 at 1:36 UTC. From left to right: Swarm B, A, and C, showing the filtered series of the magnetic field magnitude data (top panels), their corresponding wavelet spectra for the joined Pc3 and Pc4 range (middle panels), and a composite plot of the measured electron density data (green line) and their location at magnetic latitude (blue line) from -90° to $+90^{\circ}$ (bottom panels). Please note that, at the bottom of these plots, we provide information on UT, geographic longitude, and magnetic local time (MLT).

References

1. Friis-Christensen, E.; Lühr, H.; Hulot, G. Swarm: "A constellation to study the Earth's magnetic field". *Earth Planets Space* **2006**, *58*, 351–358. [CrossRef]
2. Balasis, G.; Papadimitriou, C.; Daglis, I.A.; Pilipenko, V. ULF wave power features in the topside ionosphere revealed by Swarm observations. *Geophys. Res. Lett.* **2015**, *42*, 6922–6930. [CrossRef]
3. Papadimitriou, C.; Balasis, G.; Daglis, I.A.; Giannakis, O. An initial ULF wave index derived from 2 years of Swarm observations. *Ann. Geophys.* **2018**, *36*, 287–299. [CrossRef]
4. Balasis, G.; Daglis, I.A.; Georgiou, M.; Papadimitriou, C.; Haagmans, R. Magnetospheric ULF wave studies in the frame of Swarm mission: A time–frequency analysis tool for automated detection of pulsations in magnetic and electric field observations. *Earth Planets Space* **2013**, *65*, 1385–1398. [CrossRef]
5. Stolle, C.; Lühr, H.; Rother, M.; Balasis, G. Magnetic signatures of equatorial spread F as observed by the CHAMP satellite. *J. Geophys. Res.* **2006**, *111*, A02304. [CrossRef]
6. Ghadjari, H.; Knudsen, D.; Skone, S. Standing Alfvén waves within equatorial plasma bubbles. *Geophys. Res. Lett.* **2022**, *49*, e2021GL097526. [CrossRef]
7. Spogli, L.; Alfonsi, L.; Cesaroni, C. Stepping into an equatorial plasma bubble with a Swarm overfly. *Space Weather* **2023**, *21*, e2022SW003331. [CrossRef]
8. Reddy, S.A.; Forsyth, C.; Aruliah, A.; Smith, A.; Bortnik, J.; Aa, E.; Kataria, D.O.; Lewis, G. Predicting Swarm equatorial plasma bubbles via machine learning and Shapley values. *J. Geophys. Res. Space Phys.* **2023**, *128*, e2022JA031183. [CrossRef]
9. Stolle, C.; Siddiqui, T.A.; Schreiter, L.; Das, S.K.; Rusch, I.; Rother, M.; Doornbos, E. An empirical model of the occurrence rate of low latitude post-sunset plasma irregularities derived from CHAMP and Swarm magnetic observations. *Space Weather* **2024**, *22*, e2023SW003809. [CrossRef]
10. Fraser-Smith, A.C.; Bernardi, A.; McGill, P.R.; Ladd, M.E.; Helliwell, R.A.; Villard, O.G. Low-frequency magnetic field measurements near the epicenter of the Ms 7.1 Loma Prieta earthquake. *Geophys. Res. Lett.* **1990**, *17*, 1465–1468. [CrossRef]
11. Hayakawa, M.; Kawate, R.; Molchanov, O.A.; Yumoto, K. Results of ultra-low-frequency magnetic field measurements during the Guam earthquake of 8 August 1993. *Geophys. Res. Lett.* **1996**, *23*, 241–244. [CrossRef]
12. Hayakawa, M.; Schekotov, A.; Potirakis, S.; Eftaxias, K. Criticality features in ULF magnetic fields prior to the 2011 Tohoku earthquake. *Proc. Jpn. Acad. Ser. B Phys. Biol. Sci.* **2015**, *91*, 25–30. [CrossRef] [PubMed]
13. Contoyiannis, Y.; Potirakis, S.M.; Eftaxias, K.; Hayakawa, M.; Schekotov, A. Intermittent criticality revealed in ULF magnetic fields prior to the 11 March 2011 Tohoku earthquake (Mw = 9). *Physica A* **2016**, *452*, 19–28. [CrossRef]
14. Lazaridou-Varotsos, M.S. *Earthquake Prediction by Seismic Electric Signals. The Success of the VAN Method Over Thirty Years*; Springer: Berlin/Heidelberg, Germany, 2013. [CrossRef]
15. Han, P.; Zhuang, J.; Hattori, K.; Chen, C.-H.; Febriani, F.; Chen, H.; Yoshino, C.; Yoshida, S. Assessing the potential earthquake precursory information in ULF magnetic data recorded in Kanto, Japan during 2000–2010: Distance and magnitude dependences. *Entropy* **2020**, *22*, 859. [CrossRef]
16. Schekotov, A.; Chebrov, D.; Hayakawa, M.; Belyaev, G.; Berseneva, N. Short-term earthquake prediction in Kamchatka using low-frequency magnetic fields. *Nat. Hazards* **2020**, *100*, 735–755. [CrossRef]
17. Hayakawa, M.; Schekotov, A.; Izutsu, J.; Nickolaenko, A.P.; Hobara, Y. Seismogenic ULF/ELF wave phenomena: Recent advances and future perspectives. *Open J. Earthq. Res.* **2023**, *12*, 45–113. [CrossRef]
18. Potirakis, S.M.; Contoyiannis, Y.; Schekotov, A.; Eftaxias, K.; Hayakawa, M. Evidence of critical dynamics in various electromagnetic precursors. *Eur. Phys. J. Spec. Top.* **2021**, *230*, 151–177. [CrossRef]
19. Malkotsis, P.; Papadopoulos, N.; Politis, D.Z.; Dimakos, D.; Exarhos, M.; Liadopoulos, E.; Contoyiannis, Y.; Charitopoulos, A.; Kontakos, K.; Koulouras, G.; et al. ELSEM-Net, a network of ground-based telemetric stations for the monitoring of fracture-induced electromagnetic emissions in Greece: Instrumentation, management and analysis of recent observations associated with strong earthquakes. *Ann. Geophys.* **2023**, *66*, SE638. [CrossRef]
20. Potirakis, S.M.; Contoyiannis, Y. Indications for an alternative breaking of symmetry in fracture-induced electromagnetic emissions recorded prior to the 2023 Mw7.8 and Mw7.5 Turkey Earthquakes. *Phys. A* **2024**, *639*, 129685. [CrossRef]
21. Hayakawa, M.; Kasahara, Y.; Nakamura, T.; Muto, F.; Horie, T.; Maekawa, S.; Hobara, Y.; Rozhnoi, A.A.; Solovieva, M.; Molchanov, O.A.; et al. A statistical study on the correlation between lower Ionospheric perturbations as seen by subionospheric VLF/LF propagation and earthquakes. *J. Geoph. Res.* **2010**, *115*, A09305. [CrossRef]
22. Politis, D.Z.; Potirakis, S.M.; Contoyiannis, Y.; Potamitis, I.; Sasmal, S.; Yang, S.-S.; Hayakawa, M. Lower-ionosphere anomalies prior to strong earthquakes that occurred in north-central mainland Greece on March 2021 as revealed by multi-method analysis of VLF sub-ionospheric propagation data. *Ann. Geophys.* **2023**, *66*, SE645. [CrossRef]
23. Pulinets, S.; Krankowski, A.; Hernandez-Pajares, M.; Marra, S.; Cherniak, I.; Zakharenkova, I.; Rothkaehl, H.; Kotulak, K.; Davidenko, D.; Blaszkiewicz, L.; et al. Ionosphere sounding for pre-seismic anomalies identification (INSPIRE): Results of the project and perspectives for the short-term earthquake forecast. *Front. Earth Sci.* **2021**, *9*, 610193. [CrossRef]
24. Blaunstein, N.; Hayakawa, M. Short-term ionospheric precursors of earthquakes using vertical and oblique ionosondes. *Phys. Chem. Earth* **2009**, *34*, 496–507. [CrossRef]
25. Balasis, G.; Mandea, M. Can electromagnetic disturbances related to the recent great earthquakes be detected by satellite magnetometers? *Tectonophysics* **2007**, *431*, 173–195. [CrossRef]

26. Walker, S.N.; Kadirkamanathan, V.; Pokhotelov, O.A. Changes in the ultra-low frequency wave field during the precursor phase to the Sichuan earthquake, DEMETER observations. *Ann. Geophys.* **2013**, *31*, 1597–1603. [CrossRef]
27. De Santis, A.; Balasis, G.; Pavón-Carrasco, F.J.; Cianchini, G.; Mandea, M. Potential earthquake precursory pattern from space: The 2015 Nepal event as seen by magnetic Swarm satellites. *Earth Planet. Sci. Lett.* **2017**, *461*, 119–126. [CrossRef]
28. De Santis, A.; Marchetti, D.; Pavón-Carrasco, F.J.; Cianchini, G.; Perrone, L.; Abbattista, C.; Alfonsi, L.; Amoruso, L.; Campuzano, S.A.; Carbone, M.; et al. Precursory worldwide signatures of earthquake occurrences on Swarm satellite data. *Sci. Rep.* **2019**, *9*, 20287. [CrossRef]
29. Rikitake, T. Earthquake precursors in Japan: Precursor time and detectability. *Tectonophysics* **1987**, *136*, 265–282 [CrossRef]
30. De Santis, A.; Cianchini, G.; Marchetti, D.; Piscini, A.; Sabbagh, D.; Perrone, L.; Campuzano, S.A.; Inan, S. A Multiparametric Approach to Study the Preparation Phase of the 2019 M7.1 Ridgecrest (California, United States) Earthquake. *Front. Earth Sci.* **2020**, *8*, 540398. [CrossRef]
31. INGV Working Group on the Amatrice Earthquake. Second Summary Report on the M6.0 Amatrice Earthquake of August 24, 2016 (Central Italy). 2016. Available online: https://zenodo.org/records/166241 (accessed on 6 September 2024).
32. Knudsen, D.J.; Burchill, J.K.; Buchert, S.C.; Eriksson, A.I.; Gill, R.; Wahlund, J.-E.; Åhlen, L.; Smith, M.; Moffat, B. Thermal ion imagers and Langmuir probes in the Swarm electric field instruments. *J. Geophys. Res. Space Phys.* **2017**, *122*, 2655–2673. [CrossRef]
33. Jenner, M.; Coïsson, P.; Hulot, G.; Buresova, D.; Truhlik, V.; Chauvet, L. Total root electron content: A new metric for the ionosphere below low Earth orbiting satellites. *Geophys. Res. Lett.* **2024**, *51*, e2024GL110559. [CrossRef]
34. Borovsky, J.E.; Shprits, Y.Y. Is the Dst index sufficient to define all geospace storms? *J. Geophys. Res. Space Phys.* **2017**, *122*, 11–543. [CrossRef]
35. Finlay, C.; Kloss, C.; Olsen, N.; Hammer, M.D.; Toffner-Clausen, L.; Grayver, A.; Kushinov, A. The CHAOS-7 geomagnetic field model and observed changes in the South Atlantic Anomaly. *Earth Planets Space* **2020**, *72*, 156. [CrossRef] [PubMed]
36. Katsavrias, C.; Papadimitriou, C.; Hillaris, A.; Balasis, G. Application of Wavelet Methods in the Investigation of Geospace Disturbances: A Review and an Evaluation of the Approach for Quantifying Wavelet Power. *Atmosphere* **2022**, *13*, 499. [CrossRef]
37. Potirakis, S.M.; Contoyiannis, Y.; Schekotov, A.; Asano, T.; Hayakawa, M. Analysis of the ultra-low frequency magnetic field fluctuations prior to the 2016 Kumamoto (Japan) earthquakes in terms of the method of critical fluctuations. *Physica A* **2019**, *514*, 563–572. [CrossRef]
38. Korsunova, L.P.; Khegai, V.V. Analysis of seismoionospheric disturbances at the chain of Japanese stations for vertical sounding of the Ionosphere. *Geomagn. Aeron.* **2008**, *48*, 392–399. [CrossRef]
39. Marchetti, D.; Akhoondzadeh, M. Analysis of Swarm satellites data showing seismo-ionospheric anomalies around the time of the strong Mexico (Mw = 8.2) earthquake of 08 September 2017. *Adv. Space Res.* **2018**, *62*, 614–623. [CrossRef]
40. Akhoondzadeh, M.; De Santis, A.; Marchetti, D.; Piscini, A.; Cianchini, G. Multi precursors analysis associated with the powerful Ecuador (MW = 7.8) earthquake of 16 April 2016 using Swarm satellites data in conjunction with other multi-platform satellite and ground data. *Adv. Space Res.* **2018**, *61*, 248–263. [CrossRef]
41. De Santis, A.; Marchetti, D.; Spogli, L.; Cianchini, G.; Pavón-Carrasco, F.J.; Franceschi, G.D.; Di Giovambattista, R.; Perrone, L.; Qamili, E.; Cesaroni, C.; et al. Magnetic Field and Electron Density Data Analysis from Swarm Satellites Searching for Ionospheric Effects by Great Earthquakes: 12 Case Studies from 2014 to 2016. *Atmosphere* **2018**, *10*, 371. [CrossRef]
42. Marchetti, D.; De Santis, A.; D'Arcangelo, S.; Poggio, F.; Jin, S.; Piscini, A.; Campuzano, S.A. Magnetic Field and Electron Density Anomalies from Swarm Satellites Preceding the Major Earthquakes of the 2016–2017 Amatrice-Norcia (Central Italy) Seismic Sequence. *Pure Appl. Geoph.* **2019**, *177*, 305–319. [CrossRef]
43. Akhoondzadeh, M.; De Santis, A.; Marchetti, D.; Piscini, A.; Jin, S. Anomalous seismo-LAI variations potentially associated with the 2017 Mw = 7.3 Sarpol-e Zahab (Iran) earthquake from Swarm satellites, GPS-TEC and climatological data. *Adv. Space Res.* **2019**, *64*, 143–158. [CrossRef]
44. Marchetti, D.; De Santis, A.; Campuzano, S.A.; Soldani, M.; Piscini, A.; Sabbagh, D.; Cianchini, G.; Perrone, L.; Orlando, M. Swarm Satellite Magnetic Field Data Analysis Prior to 2019 Mw = 7.1 Ridgecrest (California, USA) Earthquake. *Geosciences* **2020**, *10*, 502. [CrossRef]
45. Sasmal, S.; Chowdhury, S.; Kundu, S.; Politis, D.Z.; Potirakis, S.M.; Balasis, G.; Hayakawa, M.; Chakrabarti, S.K. Pre-Seismic Irregularities during the 2020 Samos (Greece) Earthquake (M = 6.9) as Investigated from Multi-Parameter Approach by Ground and Space-Based Techniques. *Atmosphere* **2021**, *12*, 1059. [CrossRef]
46. Akhoondzadeh, M.; De Santis, A.; Marchetti, D.; Shen, X. Swarm-TEC Satellite Measurements as a Potential Earthquake Precursor Together With Other Swarm and CSES Data: The Case of Mw7.6 2019 Papua New Guinea Seismic Event. *Front. Earth Sci. Sec. Geohazards Georisks* **2022**, *10*, 820189. [CrossRef]
47. Ghamry, E.; Mohamed, E.K.; Sekertekin, A.; Fathy, A. Integration of multiple earthquakes precursors before large earthquakes: A case study of 25 April 2015 in Nepal. *J. Atmos. Sol.-Terr. Phys.* **2023**, *242*, 105982. [CrossRef]
48. Zhang, X.; Liu, J.; De Santis, A.; Perrone, L.; Xiong, P.; Zhang, X.; Du, X. Lithosphere-atmosphere-ionosphere coupling associated with four Yutian earthquakes in China from GPS TEC and electromagnetic observations onboard satellites. *J. Geodyn.* **2023**, *155*, 101943. [CrossRef]
49. Zhang, X.; De Santis, A.; Liu, J.; Campuzano, S.A.; Yang, N.; Cianchini, G.; Ouyang, X.; D'Arcangelo, S.; Yang, M.; De Caro, M.; et al. Pre-Earthquake Oscillating and Accelerating Patterns in the Lithosphere–Atmosphere–Ionosphere Coupling (LAIC) before the 2022 Luding (China) Ms6.8 Earthquake. *Remote Sens.* **2024**, *16*, 2381. [CrossRef]

50. Ozsoz, I.; Pamukçu, O.A.; Timoçin, E. Time-dependent magnetic anomaly variations in Turkey and Greece using swarm satellites: A comprehensive precursory multi-track analysis of M $\geq$ 6 earthquakes from 2017 to 2020. *J. Atm. Solar-Terr. Phys.* **2024**, *258*, 106210. [CrossRef]
51. Heki, K. Ionospheric disturbances related to earthquakes. In *Space Physics and Aeronomy Collection, Volume 3: Ionosphere Dynamics and Applications, Geophysical Monograph 260*; Huang, C., Lu, G., Eds.; Wiley & Sons, Inc.: Hoboken, NJ, USA, 2021. [CrossRef]